Original Article

Correlation analysis of positron emission tomography/computed tomography-magnetic resonance imaging of cannabinoid type 1 receptor in the lumbar spine and brain of aged osteoporosis female cynomolgus monkeys

Lu Hou[1], Haitong Zhang[2], Ying Li[1], Honghao Zhu[1], Kai Liao[1], Bin Guo[1], Chenchen Dong[1], Guocong Li[1], Weijian Ye[1], Lu Wang[1], Hao Xu[1]

[1]Department of Nuclear Medicine, The First Affiliated Hospital of Jinan University, Guangzhou, China; [2]Department of Cardiology, Third Affiliated Hospital of Sun Yat-sen University, Guangzhou, China

Contributions: (I) Conception and design: H Xu, L Wang; (II) Administrative support: B Guo, W Ye; (III) Provision of study materials or patients: H Zhu, G Li; (IV) Collection and assembly of data: L Hou, Y Li, K Liao; (V) Data analysis and interpretation: L Hou, H Zhang, C Dong; (VI) Manuscript writing: All authors; (VII) Final approval of manuscript: All authors.

Correspondence to: Hao Xu, MD, PhD; Lu Wang, MD, PhD. Department of Nuclear Medicine, The First Affiliated Hospital of Jinan University, No. 613 West Huangpu Avenue, Guangzhou 510630, China. Email: txh@jnu.edu.cn; l_wang1009@foxmail.com.

Background: Although cannabinoid receptor 1 (CB1R) antagonists can inhibit bone loss in osteoporosis mouse models, different strains of mice show different bone mass phenotypes after knock out the *CB1R* gene. The relationship between CB1R and bone metabolism is complex, and its regulatory role in bone metabolism and as a therapeutic target for osteoporosis requires further investigation.

Methods: Based on lumbar spine volumetric bone mineral density (vBMD) data of healthy female cynomolgus monkeys aged 1–25 years, naturally aged postmenopausal female osteoporotic monkeys and normal young monkeys were screened by detecting lumbar vertebrae vBMD and estradiol levels in this study. Positron emission tomography-computed tomography (PET/CT) and magnetic resonance imaging (MRI) scans were performed on the lumbar spine and brain of the two groups of monkeys using the probe [^{11}C]OMAR, which specifically targets CB1R, and the difference in the CB1R expression of osteoporotic monkeys was evaluated.

Results: The vBMD values of two standard deviations (SDs) below the peak bone value (428.1±53.8 g/cm^3) were set as the reference standard for osteoporosis vBMD. Of the 49 healthy female cynomolgus monkeys, 4 postmenopausal older osteoporotic monkeys (18–26 years) and 5 young control monkeys (6–7 years) were selected, and the mean vBMD of the lumbar spine of the two groups was 295.07±19.11 and 419.72±16.14 g/cm^3, respectively (P<0.0001). Radioactive uptake in the lumbar spine was linearly and negatively correlated with vBMD (r=–0.7977; P=0.01). Dynamic PET/MR imaging of the brains showed that CB1R was upregulated in the osteoporosis group, and there was a negative linear correlation between the vBMD and area under the time-radioactivity curve (AUC) of the thalamus (r=–0.8506; P=0.0153) and prefrontal cortex (r=–0.8306; P=0.0207).

Conclusions: In this study, PET/CT-MRI molecular imaging technology revealed that CB1R was upregulated in the lumbar spine and brain of the osteoporosis monkeys and that CB1R may be regulated by the brain-bone axis. CB1R antagonist may be a potential drug for the treatment of osteoporosis.

Keywords: Volumetric bone mineral density (vBMD); cannabinoid receptor 1 (CB1R); osteoporotic; positron emission tomography/computed tomography-magnetic resonance imaging (PET/CT-MRI)

Submitted Feb 01, 2023. Accepted for publication Sep 14, 2023. Published online Nov 09, 2023.
doi: 10.21037/qims-23-118
View this article at: https://dx.doi.org/10.21037/qims-23-118

Introduction

Osteoporosis is a common systemic bone disease characterized by low bone mass, damage to the microstructure of bone tissue, increased bone fragility, and fracture. Osteoporosis fractures are one of the important causes of disability and death in older adult patients (1), and research shows that after 1 year of hip fracture in these patients, the mortality rates for males and females are as high as 37% and 25%, respectively (2,3). With the anticipated aging of the global population, osteoporosis has become an important public health problem in many countries. Interestingly, researchers have found that osteoporosis may not only be associated with advance age; indeed, the clinical fracture rate ratio appears to be significantly increased among people with long-term cannabis use compared to cigarette smokers (1 *vs.* 2.17; P<0.005). Moreover, compared with that in cigarette smokers, the Z value of heavy cannabis users, in either their spine or total hip score, is significantly decreased (spine: Z=0.0±1.2 *vs.* Z=–0.5±1.2, P<0.005; hip: Z=0.3±0.9 *vs.* Z=–0.2±0.9, P<0.005) (4).

There are a variety of endocannabinoids in a human body that are recognized by cannabinoid receptors, with cannabinoid receptor 1 (CB1R) being one of the most important receptors in the cannabinoid system. CB1R belongs to the G-protein-coupled receptor superfamily, which is abundantly expressed *in vivo*, particularly in the basal ganglia, cerebellum, and hippocampus of the central nervous system (CNS) (5,6). The disorders of CB1R are related to the occurrence and development of various diseases, such as obesity, addictive diseases, schizophrenia, pain, osteoporosis, and tumors (7-9). CB1R is also expressed in osteoblasts, osteoclasts, and adipocytes in the bone marrow and affects bone metabolism by modulating their function (10-12). In addition, the sympathetic expression of CB1R in bone affects bone metabolism by regulating the level of norepinephrine (13,14). The cannabinoid system in the CNS also plays a role in the regulation of bone metabolism (15,16). However, the role of CB1R in bone metabolism requires further research. Studies in rodents date back to 2005, and Idris *et al.* found that the bone mineral density (BMD) of CD1 $CB1^{-/-}$ mice was significantly higher than that of wild-type mice of the same age, and the use of the CB1R antagonist AM251 to treat ovariectomized C57 mice effectively inhibited bone loss caused by oophorectomy (17). However, Tam *et al.* found that in C57 $CB1^{-/-}$, the BMD of both male and female mice was lower than that of the wild-type mice of the same age (13). As the results regarding the role of CB1R in osteoporosis are inconsistent, the treatment potential of CB1R antagonists in osteoporosis is unclear. However, two later studies suggested that the difference in the genetic background of mice is the main reason for these discrepant results (10,13). Some studies have also indicated that the effects of CB1R agonists and antagonists on bones are related to age (10,18). Therefore, the mechanism of action of CB1R in bone is extremely complicated (9,19,20).

As the physiological structures of mice and humans differ considerably and as there is substantial variability in genetic backgrounds of different mouse strains, further clinical translation is relatively challenging. Nonhuman primates (NHPs) include those species that are most genetically similar to humans. Thus far, few studies on osteoporosis in NHPs have been conducted, and there is a lack of standard assessment for osteoporotic NHP models. Based on the results of our previous volumetric bone mineral density (vBMD) and serological studies on female cynomolgus monkeys of different age groups (21,22), a simple screening criterion for nonsurgical (natural postmenopausal) osteoporosis monkey model was established.

We used positron emission tomography (PET), a highly sensitive and specific noninvasive imaging technique. The ligands are labelled with radioisotopes as tracers and the changes in the levels of target molecules *in vivo* can be displayed in real time without producing pharmacological effects. PET can achieve quantitative acquisition of target information and has an irreplaceable role in examining disease mechanisms, revealing pharmacokinetics, and evaluating efficacy (23). In the present study, the lumbar spine of normal young and osteoporotic cynomolgus monkeys was imaged using a specific CB1R-targeting radio probe, [^{11}C]OMAR (24), which can assess the expression of CB1R in the bone. We also performed CB1R imaging of the brain to determine the connection between the

bone and brain. This investigation serves as a foundation for further exploration into the therapeutic potential of targeting CB1R in the context of osteoporotic conditions. We present this article in accordance with the ARRIVE reporting checklist (available at https://qims.amegroups.com/article/view/10.21037/qims-23-118/rc).

Methods

Animals

In this study, 29 healthy young female cynomolgus monkeys (6–10 years old) and 20 older cynomolgus monkeys (>18 years old) that had been nulliparous for at least 3 years were included. Experimental monkeys were provided by Guangdong Landau Biotechnology Co., Ltd., a company accredited by the Association for Assessment and Accreditation of Laboratory Animal Care International (AAALAC). The general health of all cynomolgus monkeys was evaluated before the experiment. Pregnant or menstruating cynomolgus monkeys and those with obvious organic lesions were excluded. The study was performed under a project license (No. LDIACUC2018-0004) granted by the Laboratory Animal Ethics Committee of Guangdong Landau Biotechnology Co., Ltd. and in compliance with the AAALAC guidelines for the care and use of animals. This study was conducted at the Department of Nuclear Medicine, First Affiliated Hospital of Jinan University. Anesthesia, blood collection, and other procedures involving the experimental monkeys were carried out by qualified veterinarians employed by the company.

Screening of experimental monkeys

Detection of serological indicators of cynomolgus monkeys

After the primary screening, 4 mL of blood was collected from each cynomolgus monkey, and then the supernatant was collected. The levels of sex hormones were detected using chemiluminescence, and the method was consistent with that previously published by our research group (21). The estrogen (E2) level of the youth group was required to be higher than or within the reported E2 levels of the corresponding age group (≥67.46±14.92 ng/mL). The E2 level of the osteoporosis group was required to be lower than or within the reported E2 level of the corresponding older group (≤49.93±9.10 ng/mL) (21); additionally, serum calcium (Ca) and phosphorus (P) levels were analyzed.

Quantitative CT (QCT) scanning of the lumbar vertebrae of cynomolgus monkeys

Lumbar spine QCT scans were performed on cynomolgus monkeys that met the above requirements for serological examination, and the scanning and analysis methods were consistent those of a previous study (22). Briefly, the vBMD of L2–4 vertebrae was measured using the three-dimensional (3D) spine module in QCT Pro Software (Mindways Software). If any of the L2–4 vertebral bodies had unevenly increased bone density or flattened vertebral bodies, three adjacent vertebral bodies in the L1–7 vertebrae were selected for vBMD measurement, and the average value of each vertebral body was measured twice. Presently, the criteria for diagnosing osteoporosis in NHPs remain undefined. Based on the previous findings concerning the BMD of cynomolgus monkeys across various age groups, it has been observed that the changes in lumbar vBMD conform to a normal distribution. In statistical analysis, a deviation of two standard deviations (SDs) from the mean is commonly used as the threshold for determining statistical significance. Therefore, in this study, the standard BMD in older osteoporotic cynomolgus monkeys was defined as two SDs below the mean peak vBMD (428.05±53.75 mg/cm^3) (22).

Synthesis of CB1R-targeting PET probe [11C]OMAR and PET/CT-MRI scanning in cynomolgus monkeys

We performed the automatic radiosynthesis of [^{11}C]OMAR on a TracerLab FX2C module (GE HealthCare) using the reaction condition reported by Fan *et al.* (25). The product was purified via high-performance liquid chromatography (HPLC) and formulated into sterile water to prepare an injection containing 10% ethanol. HPLC was used for quality control before each injection, and the radiochemical purity of the drug was >99%.

Experimental monkeys were fasted for at least 4 h before PET/CT scanning, and 10 mg/kg of ketamine was administered intramuscularly for anesthesia before scanning. [^{11}C]OMAR was slowly injected intravenously under standardized injection conditions (supine, low ambient noise, dimly lit room), with an average of 137 MBq (range, 111–185 MBq) per monkey. One-bed static lumbar spine PET/CT scans (spatial resolution of 4–5 mm) on a Discovery 690 Elite system (GE HealthCare) were performed on experimental monkeys 20 min after injection. The scanning parameters were set as previously described (26), and the acquisition time was 20 min. The imaging sequence of monkeys was consistent with

Table 1 Basic information of the experimental monkeys

No.	Age (years)	Weight (kg)	vBMD (g/cm^3)	E2 (ng/mL)	Ca (mmol/L)	P (mmol/L)
1	18	4.15	268.69	56.84	2.2	1.71
2	20	3.25	310.43	31.62	2.07	1.8
3[a]	19	4.8	307.75	13.15	2.12	1.87
4	26	3.04	293.41	11.64	2.47	0.76
5	7	3.4	393.35	87.39	1.98	1.99
6	7	3.6	418.46	97.21	2.2	1.25
7	7	3.5	435.18	72.1	2.49	1.58
8	6	3.4	429.77	114.75	2.47	1.33
9[a]	6	4.1	421.85	132.76	2.44	1.4

[a], cynomolgus monkeys did not undergo positron emission tomography/computed-magnetic resonance imaging head scans. vBMD, volumetric bone mineral density; E2, estrogen; Ca, calcium; P, phosphorus.

the order of the screening for inclusion. Some monkeys also underwent dynamic 60-min PET/CT and T1-weighted MRI head scans on a Discovery 750 system (GE HealthCare) (*Table 1*). Experimental monkeys were subjected to head PET/CT under isoflurane anesthesia with endotracheal intubation, and PET images of monkey brains were collected at the same time as the intravenous administration. The interval between two PET/CT scans was at least 3 days.

Image processing and statistical analysis of data

The fusion of MRI and PET/CT images (PET/MRI) for the brain images was completed, and the PET/CT and PET/MRI image data were processed using PMOD v. 4.1 software. The region of interest (ROI) in the lumbar spine of young cynomolgus monkeys was selected from the L2–7 vertebrae. The delineation of the ROI of the lumbar spine in aged cynomolgus monkeys was consistent with the lumbar spine measured via QCT. Dynamic PET/MRI data analysis was consistent with a previously reported method (27). All brain regions were delineated automatically from the monkey brain template developed by our group (26). PET image processing was performed by two specialized radiologists who were blinded to group assignment. SPSS software (version 26.0) was used to analyze all experimental data, and 2 independent samples *t*-tests were used to compare the differences between the two groups. Spearman rank correlation coefficient was used to test the correlation between data. Statistical significance was set at $P<0.05$.

Results

Screening of experimental monkeys

Based on a comprehensive evaluation of QCT and serological results, a total of 9 cynomolgus monkeys (4 naturally aged postmenopausal osteoporosis monkey models and 5 young female cynomolgus monkeys) met the bone density and serum E2 standards established by each group. These 9 monkeys were selected for subsequent experiments (*Table 1*).

All 9 experimental monkeys underwent a 20-min [^{11}C] OMAR PET/CT scan of the lumbar spine. *Figure 1* shows significant statistical differences in lumbar vBMD and serum E2 levels between the two groups of experimental monkeys ($P<0.0001$ and $P=0.002$, respectively). The average vBMD and E2 level of the cynomolgus monkeys in the young and osteoporosis group were 419.72±16.14 g/cm^3 and 100.84±23.62 ng/mL and 295.07±19.11 g/cm^3 and 28.31±21.08 ng/mL, respectively. No adverse events occurred during this study period.

Upregulation of CB1R expression in the lumbar vertebrae of osteoporotic monkeys

We used [^{11}C]OMAR (*Figure 2A*) to perform PET/CT imaging on the lumbar spine of two groups of cynomolgus monkeys, and the results showed that the standard uptake value (SUV) of the spine between the two groups was statistically different: the SUV of the lumbar spine in osteoporotic monkeys was higher than that in young

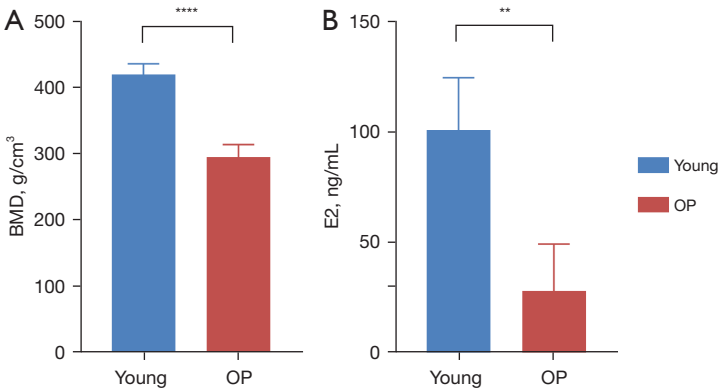

Figure 1 Comparison of lumbar vBMD and E2 level between young and OP groups of cynomolgus monkeys. (A) vBMD of the two groups of cynomolgus monkeys. (B) E2 levels of the two groups. Data are presented as the mean ± SEM. **, P<0.01; ****, P<0.0001. vBMD, volumetric bone mineral density; OP, osteoporosis; E2, estrogen; SEM, standard error of the mean.

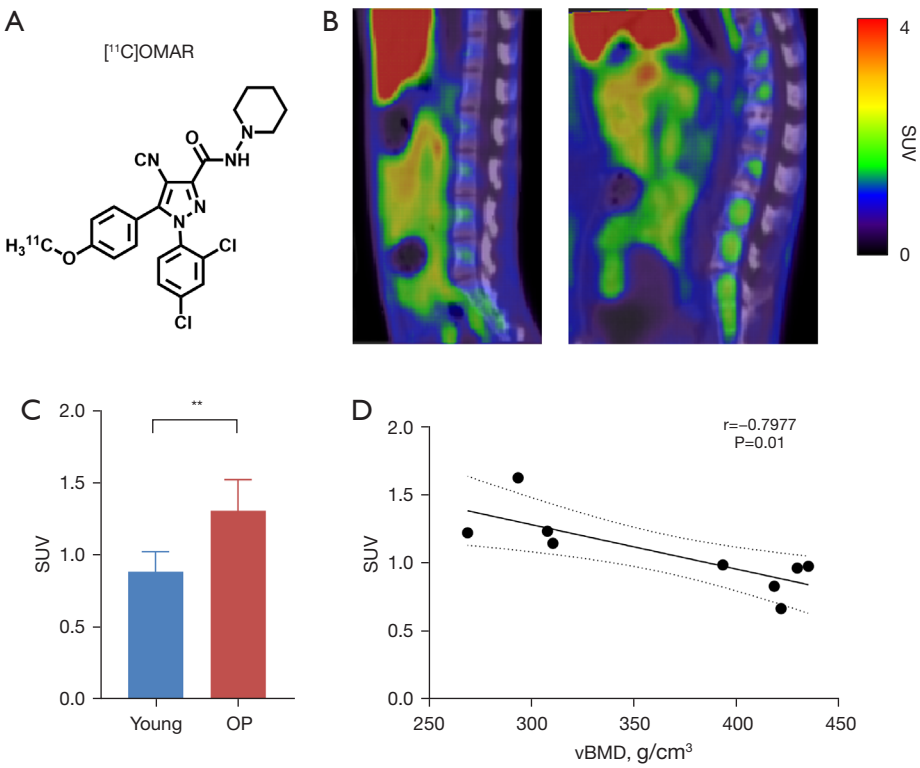

Figure 2 Static PET/CT imaging of the lumbar spine. (A) Chemical structures of [^{11}C]OMAR. (B) Static 20-min PET/CT images of the lumbar vertebrae of the two groups of cynomolgus monkeys (young group: n=5; old group: n=4). Representative images of young and older osteoporotic monkey are on the left and right side, respectively. (C) Comparison of lumbar SUV between the two groups. (D) Correlation analysis of lumbar vBMD and SUV in experimental monkeys. Data are presented as the mean ± SEM. **, P<0.01. SUV, standard uptake value; OP, osteoporosis; vBMD, volumetric bone mineral density; PET/CT, positron emission tomography/computed tomography; SEM, standard error of the mean.

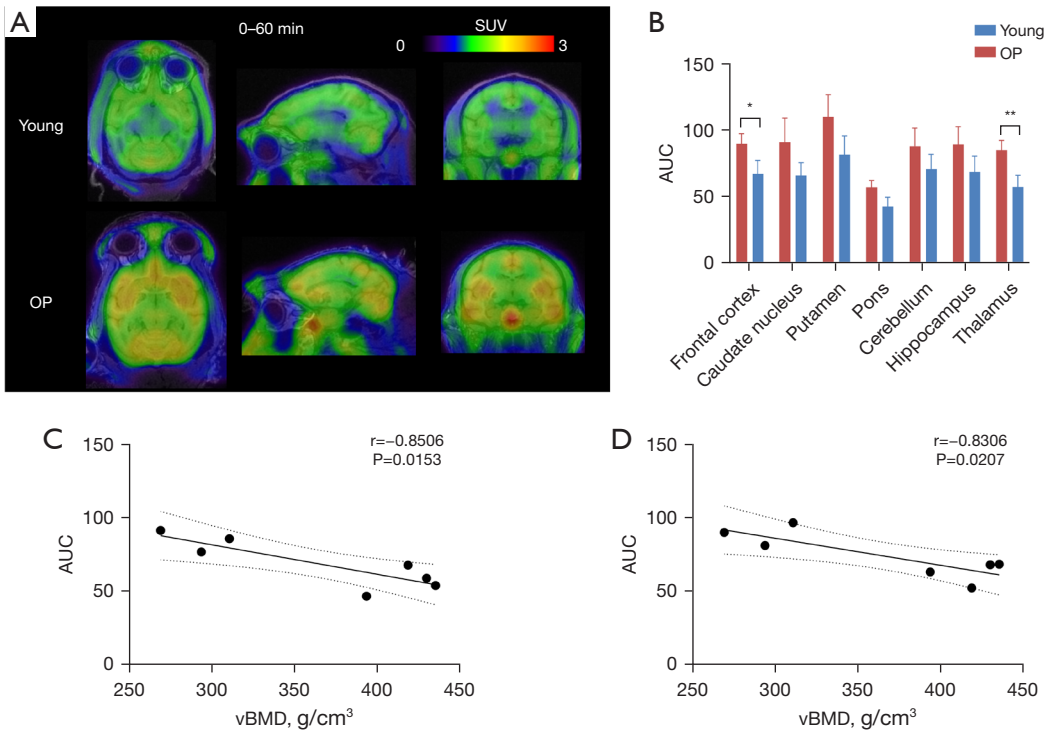

Figure 3 Dynamic 60-min PET/MRI imaging results of the monkey brain (young group: n=5; old group: n=4). (A) Representative [11C] OMAR PET/MRI images as the sum of imaging from 0 to 60 min in two groups of cynomolgus monkeys. (B) Comparison of the AUC of different brain regions in the two groups. (C) Correlation between the vBMD and AUC of the thalamus. (D) Correlation between the vBMD and AUC of the frontal cortex. Data are presented as the mean ± SEM. *, P<0.05; **, P<0.01. OP, osteoporosis; SUV, standard uptake value; AUC, area under the time-radioactivity curve; vBMD, volumetric bone mineral density; PET/MRI, positron emission tomography-magnetic resonance imaging; SEM, standard error of the mean.

monkeys (1.31±0.22 *vs.* 0.89±0.14; P=0.009; *Figure 2B,2C*). This suggested that CB1R was upregulated in the osteoporotic lumbar spine and that SUV was negatively correlated with vBMD (r=–0.7977; P=0.01; *Figure 2D*).

CB1R expression was increased in the brain of osteoporotic monkeys

Dynamic 60-min PET/CT-MRI head scans were performed on 4 young and 3 osteoporotic monkeys. In the brain regions of all cynomolgus monkeys, radiation uptake (from high to low) occurred in the putamen, caudate nucleus, cerebellum, and pons (*Figure 3A*); this is consistent with earlier imaging results in baboon and human brains (24,28). In our study, we found that the radioactive uptake in various brain regions of the osteoporotic monkeys was increased. Because of the lack of a reliable reference region for [^{11}C] OMAR (28), we calculated the area under the 60 min radioactivity curve [time-radioactivity curve (TAC)]. Although higher area under the time-radioactivity curve (AUC) values were observed in various brain areas of the osteoporosis group, statistically significant differences were only detected in the thalamus and prefrontal cortex (*Figure 3B*). To explore the relationship between vBMD and AUC values in these specific regions, we conducted a correlation analysis in the experimental monkeys. Remarkably, we identified a significant negative linear correlation between vBMD and AUC values in both the thalamus and prefrontal cortex (thalamus: r=–0.8506, P=0.0153; prefrontal cortex: r=–0.8306, P=0.0207; *Figure 3C,3D*). Thus, PET imaging data indicated that CB1R expression is upregulated in osteoporotic monkeys and not solely in the lumbar spine, but also in the thalamus and prefrontal cortex.

For the cervical spine area covered by the scan, we also analyzed the TAC of the C3–7 vertebrae in the two groups (*Figure 4A,4B*), which yielded similar results to those of the lumbar spine: the SUV (*Figure 4C*) and AUC (34.93±4.2 *vs.*

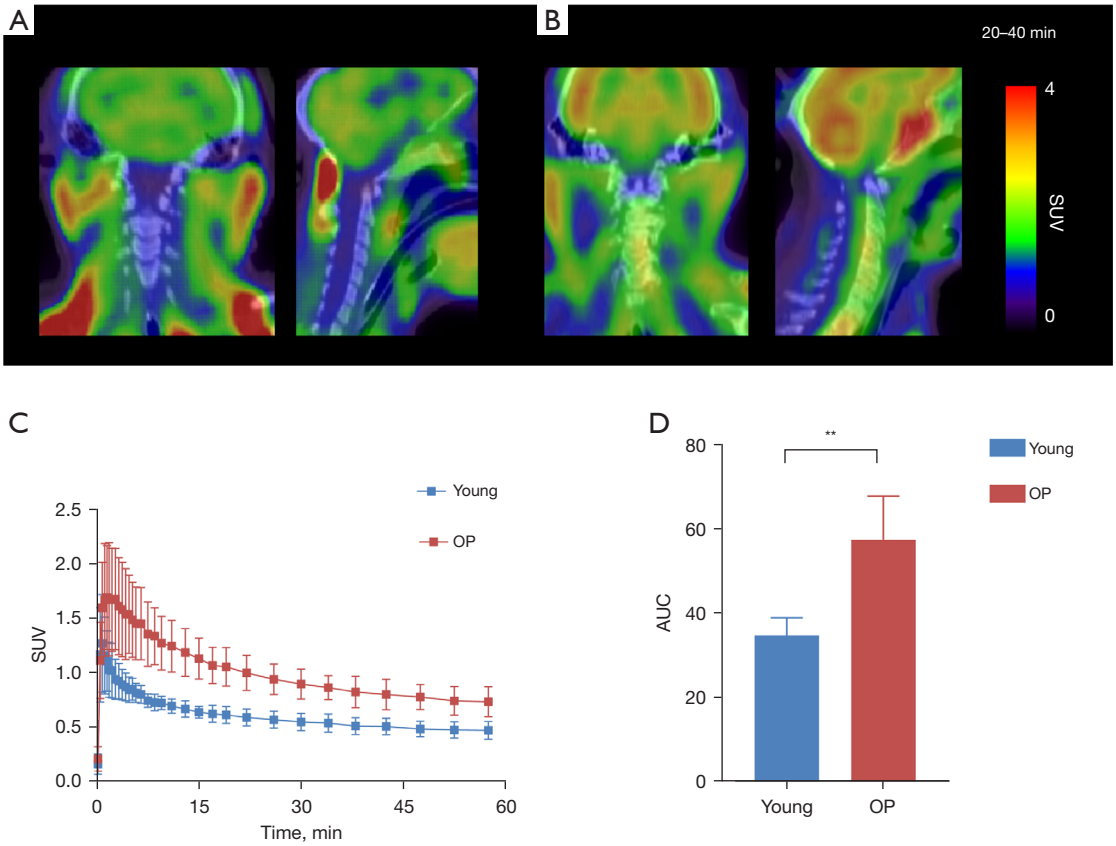

Figure 4 Dynamic 60-min PET/CT imaging results of the cervical spine. (A) Representative [^{11}C]OMAR PET/CT images as the sum of imaging from 20 to 40 min in young cynomolgus monkeys. (B) Representative [^{11}C]OMAR PET/CT images as the sum of imaging from 20 to 40 min in the osteoporotic group. (C) TAC of cervical spine PET imaging in the two groups of cynomolgus monkeys from 0 to 60 min. (D) Comparison of the AUC between the two groups. Data are presented as the mean ± SEM. **, P<0.01. SUV, standard uptake value; OP, osteoporosis; AUC, area under the TAC; PET/CT, positron emission tomography/computed tomography; TAC, time-radioactivity curve; SEM, standard error of the mean.

57.62±10.32; P=0.009; *Figure 4D*) of the osteoporotic group was higher than that of the young group.

Discussion

Screening and determination of the osteoporosis monkey model

Currently, the most common method in osteoporosis research is the establishment of a model via surgical removal of the bilateral ovary (29). However, this method is not in line with normal physiological changes, and sudden changes in hormone levels after ovariectomy in young adulthood may affect hormone-sensitive indicators. The cynomolgus monkey is a type of NHP, and its genome sequence and physiological changes are very similar to those of humans; therefore, it is more relevant as an experimental animal model than is a rodent model (30). Additionally, physiological changes in aged osteoporotic monkeys after natural menopause are similar to those in humans with osteoporotic diseases, which may be highly informative for clinical translation into therapeutic drugs.

In clinical practice, BMD is typically measured using dual-energy X-ray absorptiometry (DXA). The T value represents the number of SDs by which the BMD obtained from the DXA examination differs from the BMD of a normal young population. A T value equal to or less than –2.5 is used to diagnose osteoporosis (31), with the reference data derived from statistical results in White populations. Unlike DXA, QCT for measuring vertebral cancellous bone BMD is not influenced by factors such as height and weight,

spinal hyperplasia, degeneration, and vascular calcification (32,33). Our previous research indicated a significant presence of bone hyperplasia in aged monkeys that can substantially impact DXA measurements. Consequently, to address this issue and ensure more accurate screening of osteoporosis in our experimental monkeys, we used QCT as the preferred method for BMD assessment.

In the early stage, our group completed a large-scale measurement of vBMD and the levels of sex hormones in healthy female cynomolgus monkeys of different ages and obtained the bone growth curve of normal female cynomolgus monkeys (21,22). Hence, we were able to screen and evaluate osteoporotic monkeys in a noninvasive manner (QCT scan + measurement of serum E2 levels). This will lay the foundation for subsequent studies of osteoporotic diseases in NHPs. Although *in vitro* histological confirmation of the osteoporosis monkey model was not performed in this study, confirmation could be conducted via imaging and serological indicators. Additionally, this latter method does not require surgery, conserves manpower and material resources, and avoids animal abuse resulting from experimentation. However, a certain number of healthy female cynomolgus monkeys are required for model screening, which is an important research limitation.

In addition, we used the vBMD measured by QCT as the screening standard for the osteoporosis monkey model. This is because we found that the BMD of aged cynomolgus monkeys measured using DXA was higher than the actual value. Bone hyperplasia is almost universal in older monkeys, which greatly affects the accuracy of BMD data; therefore, to determine vBMD in aged female cynomolgus monkeys, we chose the L5–7 vertebrae (22).

The visualization of CB1R expression in bone via PET

PET is being increasingly used in the research of central or tumor diseases to study the pathophysiological changes of related diseases at the molecular level. It is also used in pharmacokinetic and target quantification studies (34-36). In bone research, the most commonly used PET probe is [^{18}F]NaF, which mainly reflects osteogenic activity and bone blood flow by replacing the hydroxyl group in the hydroxyapatite crystal and covalent binding to the newly formed bone surface (37); however, few studies have used PET/CT for specific targets on bone. [^{11}C]OMAR (developed by Horti *et al.*) (24) is a probe that specifically targets CB1R and has been used in the research of various mental and metabolic diseases (38-40). In this study, we found that the expression of CB1R in bone could be visualized with PET imaging, which lays a foundation for establishing a quantitative relationship between CB1R and advanced osteoporosis stages. This is of great significance for more comprehensively understanding the impact of cannabinoid receptors on the pathogenesis of osteoporosis and for developing targeted CB1R drugs for osteoporosis.

In recent years, a growing amount of evidence has indicated that the central neural circuit of the brain can directly influence peripheral sympathetic nerves, thereby affecting skeletal metabolism and function. One specific brain region that has been highlighted is the ventral medial hypothalamus (41,42). Recent studies have also demonstrated that increased sympathetic excitability and elevated levels of norepinephrine in bone tissue can lead to excessive production of neuropeptide Y. This enhances the adipogenic differentiation ability of bone marrow mesenchymal stem cells while weakening their osteogenesis ability. Consequently, this imbalance between bone and lipid homeostasis ultimately culminates in age-related or postmenopausal osteoporosis (43). These findings support the existence of an intricate interplay between the CNS and bone tissue, with the sympathetic nervous system emerging as a prominent regulatory mechanism governing bone metabolism. Earlier investigations employing immunohistochemistry on mouse femurs have successfully identified the expression of CB1R receptors in sympathetic nerves situated along bone trabeculae (14). It is well-established that CB1R receptors on sympathetic nerves generally inhibit the release of norepinephrine (44), which may account for the observed phenotype of enhanced bone density in CD1 CB1R$^{-/-}$ mice. Conversely, the diminished bone mass phenotype in C57 CB1R$^{-/-}$ mice might be attributed to factors such as strain variation and skeletal growth patterns, among others.

The PET imaging analysis conducted in this study revealed a significant upregulation of CB1R expression in the lumbar spine of the osteoporotic group, providing partial confirmation of the potential efficacy of CB1R antagonists for early-stage osteoporosis treatment. Moreover, an elevation in CB1R expression was observed in various brain regions of osteoporotic experimental monkeys, aligning with previous findings reported by Van Laere *et al.*, who employed a different CB1R PET probe, [^{18}F]MK9470, to image healthy volunteers across different age groups. The aforementioned study identified augmented uptake of [^{18}F]MK9470 in the brains of older women relative to

younger women, with the basal ganglia, lateral temporal cortex, and limbic system—particularly the hippocampus—demonstrating the most prominent upregulation. Researchers have postulated that this phenomenon could potentially be attributed to a compensatory mechanism in response to CB1R upregulation resulting from diminished levels of E2 (45). Quantitative studies of CB1R in the brains of castrated rats have also been conducted and have reported that CB1R is upregulated in the hippocampus of female and male rats after castration (46,47). Our study similarly revealed heightened CB1R binding in the cerebral cortex and limbic system of postmenopausal osteoporotic monkeys. However, statistically significant increases were only observed in the thalamus and prefrontal cortex. Anatomically, among the regions of the brain, neither the thalamus nor the frontal cortex is the one with the most abundant CB1R expression, and the thalamus is an important center of sensory conduction. Except for the sense of smell, the conduction pathways of various senses are replaced by neurons in the thalamus and then projected onto the cerebral cortex. Therefore, in many studies on the relationship between CB1R and pain, the regulation of CB1R in the thalamus is indispensable (48,49), and the prefrontal cortex is also involved in the regulation of pain (50). However, few studies exist linking these two regions with bone metabolism. Given the limited sample size of cynomolgus monkeys use in this study, further validation through experiments in molecular biology is warranted to consolidate the obtained results.

The potential of peripherally restricted CB1R antagonists in osteoporosis treatment

CB1R antagonists exert therapeutic effects in ovariectomized osteoporotic mice (17) or in osteoporotic rats with hypoxia (51). However, these antagonists have been typically rimonabant or its analogues, and a major drawback of these drugs is that they can cross the blood-brain barrier, causing severe side effects in the CNS (52). To circumvent this, peripherally restricted CB1R antagonists have been developed and have shown good therapeutic effect in preclinical studies of various diseases (53-55). Therefore, we believe that peripherally restricted CB1R antagonists have potential in the treatment of osteoporosis.

Conclusions

Based on previous research, we successfully developed a model of osteoporotic monkeys with natural menopause. Our molecular imaging analysis further revealed an upregulation of CB1R expression in both the lumbar spine and brain of osteoporotic monkeys. This intriguing observation suggests a potential link between the regulation of bone metabolism and CB1R expression within the brain and skeletal system. However, further experimental verification of the molecular biology is required. These findings may contribute to the clinical translation of CB1R-related drugs for osteoporosis treatment.

Acknowledgments

The authors would like to thank all participants who contributed their time and efforts to this study.

Funding: This work was supported by the National Natural Science Foundation of China (No. 81871383) and the Science and Technology Projects in Guangzhou (No. 202201020053).

Footnote

Reporting Checklist: The authors have completed the ARRIVE reporting checklist. Available at https://qims.amegroups.com/article/view/10.21037/qims-23-118/rc

Conflicts of Interest: All authors have completed the ICMJE uniform disclosure form (available at https://qims.amegroups.com/article/view/10.21037/qims-23-118/coif). The authors report that this work was supported by the National Natural Science Foundation of China (No. 81871383) and the Science and Technology Projects in Guangzhou (No. 202201020053). The authors have no other conflicts of interest to declare.

Ethical Statement: The authors are accountable for all aspects of the work in ensuring that questions related to the accuracy or integrity of any part of the work are appropriately investigated and resolved. The study was performed under a project license (No. LDIACUC2018-0004) granted by the Laboratory Animal Ethics Committee of Guangdong Landau Biotechnology Co., Ltd., and in compliance with the AAALAC guidelines for the care and use of animals.

References

1. Sànchez-Riera L, Wilson N. Fragility Fractures & Their Impact on Older People. Best Pract Res Clin Rheumatol 2017;31:169-91.
2. Kanis JA, Oden A, Johnell O, et al. The components of excess mortality after hip fracture. Bone 2003;32:468-73.
3. Kannegaard PN, van der Mark S, Eiken P, et al. Excess mortality in men compared with women following a hip fracture. National analysis of comedications, comorbidity and survival. Age Ageing 2010;39:203-9.
4. Sophocleous A, Robertson R, Ferreira NB, et al. Heavy Cannabis Use Is Associated With Low Bone Mineral Density and an Increased Risk of Fractures. Am J Med 2017;130:214-21.
5. Hou L, Rong J, Haider A, et al. Positron Emission Tomography Imaging of the Endocannabinoid System: Opportunities and Challenges in Radiotracer Development. J Med Chem 2021;64:123-49.
6. Glass M, Dragunow M, Faull RL. Cannabinoid receptors in the human brain: a detailed anatomical and quantitative autoradiographic study in the fetal, neonatal and adult human brain. Neuroscience 1997;77:299-318.
7. Borgan F, Kokkinou M, Howes O. The Cannabinoid CB(1) Receptor in Schizophrenia. Biol Psychiatry Cogn Neurosci Neuroimaging 2021;6:646-59.
8. Iannotti FA, Di Marzo V, Petrosino S. Endocannabinoids and endocannabinoid-related mediators: Targets, metabolism and role in neurological disorders. Prog Lipid Res 2016;62:107-28.
9. Saponaro F, Ferrisi R, Gado F, et al. The Role of Cannabinoids in Bone Metabolism: A New Perspective for Bone Disorders. Int J Mol Sci 2021;22:12374.
10. Idris AI, Sophocleous A, Landao-Bassonga E, et al. Cannabinoid receptor type 1 protects against age-related osteoporosis by regulating osteoblast and adipocyte differentiation in marrow stromal cells. Cell Metab 2009;10:139-47.
11. Sophocleous A, Marino S, Kabir D, et al. Combined deficiency of the Cnr1 and Cnr2 receptors protects against age-related bone loss by osteoclast inhibition. Aging Cell 2017;16:1051-61.
12. Ko JY, Wu RW, Kuo SJ, et al. Cannabinoid receptor 1 mediates glucocorticoid-induced bone loss in rats by perturbing bone mineral acquisition and marrow adipogenesis. Arthritis Rheum 2012;64:1204-14.
13. Tam J, Ofek O, Fride E, et al. Involvement of neuronal cannabinoid receptor CB1 in regulation of bone mass and bone remodeling. Mol Pharmacol 2006;70:786-92.
14. Tam J, Trembovler V, Di Marzo V, et al. The cannabinoid CB1 receptor regulates bone formation by modulating adrenergic signaling. FASEB J 2008;22:285-94.
15. Jiang H, Wu Y, Valverde P, et al. Central adiponectin induces trabecular bone mass partly through epigenetic downregulation of cannabinoid receptor CB1. J Cell Physiol 2019;234:7062-9.
16. Eger M, Bader M, Bree D, et al. Bone Anabolic Response in the Calvaria Following Mild Traumatic Brain Injury is Mediated by the Cannabinoid-1 Receptor. Sci Rep 2019;9:16196.
17. Idris AI, van 't Hof RJ, Greig IR, et al. Regulation of bone mass, bone loss and osteoclast activity by cannabinoid receptors. Nat Med 2005;11:774-9.
18. Deis S, Srivastava RK, Ruiz de Azua I, et al. Age-related regulation of bone formation by the sympathetic cannabinoid CB1 receptor. Bone 2018;108:34-42.
19. Idris AI, Ralston SH. Cannabinoids and bone: friend or foe? Calcif Tissue Int 2010;87:285-97.
20. Raphael-Mizrahi B, Gabet Y. The Cannabinoids Effect on Bone Formation and Bone Healing. Curr Osteoporos Rep 2020;18:433-8.
21. Li Y, Cai Q, Dong C, et al. Analysis of serum bone turnover markers in female cynomolgus monkeys of different ages. Front Endocrinol (Lausanne) 2022;13:984523.
22. Zeng C, Guo B, Zhang S, et al. Age-related changes in lumbar bone mineral density measured using quantitative computed tomography in healthy female cynomolgus monkeys. Quant Imaging Med Surg 2023;13:2038-52.
23. Chételat G, Arbizu J, Barthel H, Garibotto V, Law I, Morbelli S, et al. Amyloid-PET and 18F-FDG-PET in the diagnostic investigation of Alzheimer's disease and other dementias. Lancet Neurol 2020;19:951-62.
24. Horti AG, Fan H, Kuwabara H, et al. 11C-JHU75528: a radiotracer for PET imaging of CB1 cannabinoid receptors. J Nucl Med 2006;47:1689-96.
25. Fan H, Ravert HT, Holt DP, Dannals RF, Horti AG. Synthesis of 1-(2,4-dichlorophenyl)-4-cyano-5-(4-[11C] methoxyphenyl)-N-(piperidin-1-yl)-1H-pyrazole-3-

carboxamide ([11C]JHU75528) and 1-(2-bromophenyl)-4-cyano-5-(4-[11C]methoxyphenyl)-N-(piperidin-1-yl)-1H-pyrazole-3-carboxamide ([11C]JHU75575) as potential radioligands for PET imaging of cerebral cannabinoid receptor. J Label Compd Radiopharm 2006;49:1021-36.
26. Nie B, Wang L, Hu Y, et al. A population stereotaxic positron emission tomography brain template for the macaque and its application to ischemic model. Neuroimage 2019;203:116163.
27. Xiao Z, Wei H, Xu Y, et al. Discovery of a highly specific (18)F-labeled PET ligand for phosphodiesterase 10A enabled by novel spirocyclic iodonium ylide radiofluorination. Acta Pharm Sin B 2022;12:1963-75.
28. Wong DF, Kuwabara H, Horti AG, et al. Quantification of cerebral cannabinoid receptors subtype 1 (CB1) in healthy subjects and schizophrenia by the novel PET radioligand 11COMAR. Neuroimage 2010;52:1505-13.
29. Gauthier A, Kanis JA, Martin M, et al. Development and validation of a disease model for postmenopausal osteoporosis. Osteoporos Int 2011;22:771-80.
30. Tan T, Wu J, Si C, et al. Chimeric contribution of human extended pluripotent stem cells to monkey embryos ex vivo. Cell 2021;184:2020-2032.e14.
31. Wáng YXJ. The definition of spine bone mineral density (BMD)-classified osteoporosis and the much inflated prevalence of spine osteoporosis in older Chinese women when using the conventional cutpoint T-score of -2.5. Ann Transl Med 2022;10:1421.
32. Link TM, Lang TF. Axial QCT: clinical applications and new developments. J Clin Densitom 2014;17:438-48.
33. Engelke K. Quantitative Computed Tomography-Current Status and New Developments. J Clin Densitom 2017;20:309-21.
34. Bouleau A, Lebon V, Truillet C. PET imaging of immune checkpoint proteins in oncology. Pharmacol Ther 2021;222:107786.
35. Rohren EM, Turkington TG, Coleman RE. Clinical applications of PET in oncology. Radiology 2004;231:305-32.
36. Maria Moresco R, Messa C, Lucignani G, et al. PET in psychopharmacology. Pharmacol Res 2001;44:151-9.
37. Park PSU, Raynor WY, Sun Y, et al. (18)F-Sodium Fluoride PET as a Diagnostic Modality for Metabolic, Autoimmune, and Osteogenic Bone Disorders: Cellular Mechanisms and Clinical Applications. Int J Mol Sci 2021;22:6504.
38. Ranganathan M, Cortes-Briones J, Radhakrishnan R, et al. Reduced Brain Cannabinoid Receptor Availability in Schizophrenia. Biol Psychiatry 2016;79:997-1005.
39. Valenta I, Varga ZV, Valentine H, et al. Feasibility Evaluation of Myocardial Cannabinoid Type 1 Receptor Imaging in Obesity: A Translational Approach. JACC Cardiovasc Imaging 2018;11:320-32.
40. Volk DW, Eggan SM, Horti AG, et al. Reciprocal alterations in cortical cannabinoid receptor 1 binding relative to protein immunoreactivity and transcript levels in schizophrenia. Schizophr Res 2014;159:124-9.
41. Yang F, Liu Y, Chen S, et al. A GABAergic neural circuit in the ventromedial hypothalamus mediates chronic stress-induced bone loss. J Clin Invest 2020;130:6539-54.
42. Liu Y, Shao J, Gao D, et al. Astrocytes in the Ventromedial Hypothalamus Involve Chronic Stress-Induced Anxiety and Bone Loss in Mice. Neural Plast 2021;2021:7806370.
43. Zhang Y, Chen CY, Liu YW, et al. Neuronal Induction of Bone-Fat Imbalance through Osteocyte Neuropeptide Y. Adv Sci (Weinh) 2021;8:e2100808.
44. Ishac EJ, Jiang L, Lake KD, et al. Inhibition of exocytotic noradrenaline release by presynaptic cannabinoid CB1 receptors on peripheral sympathetic nerves. Br J Pharmacol 1996;118:2023-8.
45. Van Laere K, Goffin K, Casteels C, Dupont P, Mortelmans L, de Hoon J, Bormans G. Gender-dependent increases with healthy aging of the human cerebral cannabinoid-type 1 receptor binding using [(18)F]MK-9470 PET. Neuroimage 2008;39:1533-41.
46. Riebe CJ, Hill MN, Lee TT, et al. Estrogenic regulation of limbic cannabinoid receptor binding. Psychoneuroendocrinology 2010;35:1265-9.
47. Farquhar CE, Breivogel CS, Gamage TF, et al. Sex, THC, and hormones: Effects on density and sensitivity of CB(1) cannabinoid receptors in rats. Drug Alcohol Depend 2019;194:20-7.
48. Hillard CJ. Stress regulates endocannabinoid-CB1 receptor signaling. Semin Immunol 2014;26:380-8.
49. Wang H, Dong P, He C, et al. Incerta-thalamic Circuit Controls Nocifensive Behavior via Cannabinoid Type 1 Receptors. Neuron 2020;107:538-551.e7.
50. Mecca CM, Chao D, Yu G, et al. Dynamic Change of Endocannabinoid Signaling in the Medial Prefrontal Cortex Controls the Development of Depression After Neuropathic Pain. J Neurosci 2021;41:7492-508.
51. Dou ZJ, Gao XL, Jia YL, et al. CB1 receptor antagonist rimonabant protects against chronic intermittent hypoxia-induced bone metabolism disorder and destruction in rats. Sleep Breath 2020;24:1441-9.
52. Sam AH, Salem V, Ghatei MA. Rimonabant: From RIO to

Ban. J Obes 2011;2011:432607.
53. O'Sullivan SE, Yates AS, Porter RK. The Peripheral Cannabinoid Receptor Type 1 (CB(1)) as a Molecular Target for Modulating Body Weight in Man. Molecules 2021;26:6178.
54. Chen W, Shui F, Liu C, et al. Novel Peripherally Restricted Cannabinoid 1 Receptor Selective Antagonist TXX-522 with Prominent Weight-Loss Efficacy in Diet Induced Obese Mice. Front Pharmacol 2017;8:707.
55. Zhang H, Lund DM, Ciccone HA, et al. Peripherally restricted cannabinoid 1 receptor agonist as a novel analgesic in cancer-induced bone pain. Pain 2018;159:1814-23.

Cite this article as: Hou L, Zhang H, Li Y, Zhu H, Liao K, Guo B, Dong C, Li G, Ye W, Wang L, Xu H. Correlation analysis of positron emission tomography/computed tomography-magnetic resonance imaging of cannabinoid type 1 receptor in the lumbar spine and brain of aged osteoporosis female cynomolgus monkeys. Quant Imaging Med Surg 2023;13(12):7924-7935. doi: 10.21037/qims-23-118

